Microstructure and mechanical properties of physical vapor deposited Cu/W nanoscale multilayers: Influence of layer thickness and temperature

M.A. Monclús , M. Karlik , M. Callisti , E. Frutos , J. LLorca , T. Polcar , J.M. Molina-Aldareguía

A B S T R A C T

Based on our previous knowledge on Cu/Nb nanoscale metallic multilayers (NMMs), Cu/W NMMs show a good potential for applications as heat skins in plasma experiments and armors, and it could be expected that the substitution of Nb by W would increase the strength, particularly at high temperatures. To check this hypothesis, Cu/W NMMs with individual layer thicknesses ranging between 5 and 30 nm were deposited by physical vapor deposition, and their mechanical properties were measured by nanoindentation. The results showed that, contrary to Cu/Nb NMMs, the hardness was independent of the layer thickness and decreased rapidly with temperature, especially above 200 °C. This behavior was attributed to the growth morphology of the W layers as well as the jagged Cu/W interface, both a consequence of the low W adatom mobility during deposition. Therefore, future efforts on the development of Cu/W multilayers should concentrate on optimization of the W deposition parameters via substrate heating and/or ion assisted deposition to increase the W adatom mobility during deposition.

1. Introduction

Nanoscale metallic multilayers (NMMs) have been the subject of an increasing number of studies in the past 10 years due to their outstanding mechanical properties. They originate from the high density of interfaces, which change the conventional mechanisms of plastic deformation when the individual layer thickness is below ≈ 100 nm. The strength of NMMs depends on the modulation periodicity (Λ) and several mechanisms have been proposed to explain their ultra-high strength, such as: (1) coherency strain hardening [1–3], (2) structure barrier strengthening [4], (3) modulus mismatch [5,6], and (4) intermixing at the interface [7,8]. At length scales from a few tens of nm down to a few nm, the interface between adjacent layers acts as a barrier to dislocation transmission, since slip transmission resistance is higher than gliding resistance, and hence, dislocation movement is confined to isolated layers. In this case the deformation is best described by the confined layer slip mechanism [9,10]. For layer thicknesses of only a few nm, dislocation transmission across interfaces is expected to dominate the deformation mode, resulting in softening of the NMM [8,11].

From all possible metal combinations, multilayers made up of face-centered cubic (fcc) and body-centered cubic (bcc) metals, leading to NMMs with incoherent interfaces, have shown the highest room temperature strengthening [12]. Cu/Nb NMMs are one of the most studied systems in literature, but other combinations are possible. For instance, the substitution of Nb by W, to produce Cu/W NMMs, is promising. W based coatings have been recently developed for high temperature applications in the field of wear and erosion resistant components [13, 14]. On the other hand, Cu and its alloys exhibit high thermal conductivity and fracture toughness. The Cu/W system is highly immiscible due to the different crystal structure of Cu and W (fcc vs. bcc), their lattice parameter mismatch (15% difference) and their positive mixing enthalpy (+36 kJ) [15]. Thus, Cu/W interfaces are expected to be a large obstacle to dislocation transmission. Atomistic simulations suggest that this type of interface is a good sink for radiation-generated point defects [16] and Cu/W multilayers produced by magnetron sputtering have already shown good He radiation tolerance [17,18]. Therefore, Cu/W multilayers present a good potential for applications as heat skins in plasma experiments and armors [19,20].

Among the different available processing techniques, physical vapor deposition (PVD) allows the growth of NMMs with precise control of modulation periodicity. To date, only a few studies exist on the deposition

of Cu/W multilayers by PVD [21,22] and little is known about the resulting structural and mechanical properties. Moreover, nuclear materials must withstand high temperatures and stresses during operation but there is no information available up to date on the high temperature properties of Cu/W NMMs. The objective of this paper is to contribute to fill this gap by investigating the structure and hardness of PVD Cu/W NMMs as a function of modulation periodicity and temperature.

2. Experimental techniques

2.1. Materials and microstructural characterization

Three sets of Cu/W multilayers (5/5 nm, 15/15 nm and 30/30 nm) were deposited with different modulation periodicities ($\Lambda = 10$ nm, 30 nm and 60 nm with a nominal layer thickness for Cu and W of $\Lambda/2$) on single crystal (100) Si wafers using a balanced magnetron sputtering apparatus (Kurt J. Lesker Company, Pennsylvania, US). 2″ targets (Kurt J. Lesker Company) of W (99.95% purity) and Cu (99.99% purity) were used to deposit the layers. The direct current (DC) sources were located at a target-to-substrate distance of ~120 mm and were tilted about 30° to the substrate normal, in order to increase the deposition rates. The chamber was pumped down to a base pressure of 1×10^{-5} Pa, while the depositions were carried out with an Ar gas flow of 10 sccm. The substrate holder was rotated at 10 rpm during deposition to ensure composition homogeneity on the substrate. The DC power was kept constant at 110 W for copper and at 210 W for tungsten, providing deposition rates of 0.13 and 0.29 nm/s, respectively. The multilayer-type structure was obtained by automatically controlling the shutters' opening times according to the deposition rates of Cu and W. Every deposition was carried out for about 2 h, resulting in a total film thickness of ≈1.15 μm.

The microstructure was investigated by grazing incidence X-ray diffraction (XRD) and transmission electron microscopy (TEM). The XRD grazing angle was set at 5° with a scan step size of 0.02° over an angle range of $2\theta = 20$–80°. The diffraction data were collected using an X'Pert-Pro Philips diffractometer (PANalytical, ALMELO, The Netherlands) equipped with Cu Kα radiation. The XRD patterns were analyzed by using the X'Pert HighScore Plus software together with an ICDD PDF-2 database. The modulation and interface structure of the multilayers was studied by transmission electron microscope (FEI Tecnai G^2 F20 XT) operated at 200 kV accelerating voltage. Samples for TEM were prepared by cleavage of two samples (5 mm × 3 mm), which were glued together to obtain a Si-multilayer-glue-multilayer-Si sandwich. Cross-sectional samples of thickness ≈ 0.5 mm were then cut using a slow speed diamond saw. These cross-sections were then polished from one side, glued to a standard 3 mm copper washer, mechanically thinned to 20 μm, dimple polished, and ion-beam milled in a Gatan PIPS 691 device. Some TEM samples were also prepared across selected indentations to study the deformation mechanisms, using a focused ion beam (FIB) system (FEI Helios 600i). Secondary electron microscopy (SEM) images of the cross-sections were obtained using the lens detector of the FIB system with an operating voltage of 30 kV. Atomic force microscopy (AFM) analysis of the surface roughness and the residual imprints was carried out using a Park XE150 AFM Instrument (Park Systems Corp., Suwon, Korea) in non-contact mode.

2.2. Nanoindentation testing

Nanoindentation measurements were performed using a Hysitron Triboindenter TI950 Instrument (MN, USA) fitted with a diamond Berkovich tip. The indentation hardness and modulus were measured at room temperature using maximum loads of 0.5, 1, 2, 3, 4, 6 and 10 mN, with an indentation strain rate of 0.1 s^{-1}, and holding/unloading times of 5 s. Hardness and elastic modulus at each load were evaluated from the load depth indentation curves using the Oliver and Pharr method [23], assuming a Poisson ratio of 0.3 for the NMMs. The reported values are the average of twenty indents.

The hot hardness of the multilayers was measured using the Nanotest Platform 3 Instrument (Micromaterials, Wrexham, UK). The indentation chamber was filled with Ar gas until a final O_2 level of ~0.1% was reached. High temperature nanoindentation tests were performed at T = 100, 200, 300 and 350 °C. Samples were mounted on a hot stage using high temperature cement (Omegabond 400). A thermocouple was placed on the sample surface and used to match the temperature between the sample surface and the indenter tip in order to minimize thermal drift. Reported hardness values are an average of five indents performed using a maximum load of 2 mN and loading, holding and unloading times of 10, 5 and 5 s, respectively.

3. Experimental results

3.1. Microstructure

The XRD patterns of the as-deposited Cu/W multilayers are shown in Fig. 1 for $\Lambda = 60$, 30 and 10 nm. In all cases, only the bcc α-W phase and the fcc Cu phase were detected, with no traces of other phases. As expected, the peaks broadened as the periodicity decreased, owing to the Scherrer broadening.

Figs. 2 and 3 show scanning transmission electron microscopy (STEM) high-angle annular dark field (HAADF) images for the multilayers with $\Lambda = 10$ and 60 nm, respectively. The electron scattering from W atoms is stronger than that produced by Cu atoms; as a consequence the W layers appear brighter. The layered structure was well defined in all cases, but the layers, initially flat close to the Si substrate, quickly became wavy as deposition progressed. The waviness in the layers started earlier for the case $\Lambda = 10$ nm than for $\Lambda = 60$ nm. While waviness was already apparent after the deposition of the second layer for $\Lambda = 10$ nm, it was only noticeable after the fifth layer for $\Lambda = 60$ nm (Fig. 3(a)). The transition from planar to wavy interfaces seemed to be a consequence of the cumulative layer waviness developed in the multilayers and the shadowing effects inherent to sputtering processes. In other words, any local protuberance that develops at one interface becomes more pronounced in the subsequent layers, as the adatom incorporation rate at the top of the protuberance is larger than at the valleys due to shadowing effects and the limited surface adatom mobility. As a result, the multilayers developed a columnar structure, with a column width between 20 and 100 nm, with some voids developing at the columnar boundaries, as pointed by the white arrows in Fig. 2(c). The layer waviness amplitude was large enough to break up the layers

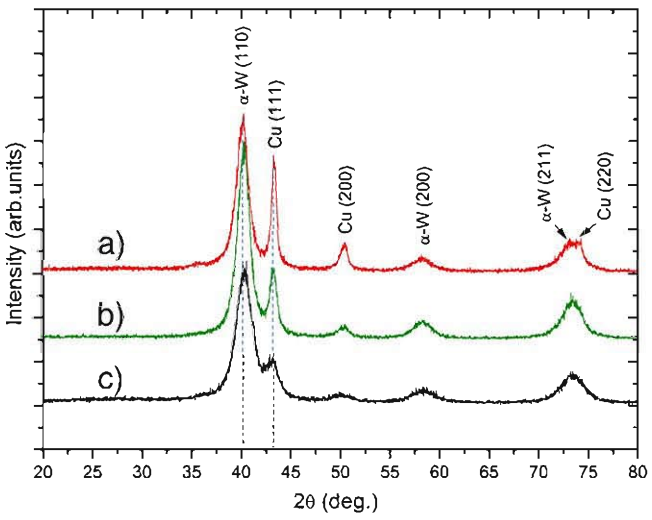

Fig. 1. XRD diffractograms of the Cu/W multilayers with the following periodicities: (a) 60 nm, (b) 30 nm and (c) 10 nm.

of the 5/5 nm multilayer, as shown in Fig. 2(d), but not the layers of the 30/30 nm multilayer.

Additionally, the STEM images manifest some important differences in the growth morphology of Cu and W. While the Cu layers were fully dense and homogeneous, the W layers display a fibrous type morphology, with thin dark "veins" oriented nearly perpendicular to the interface, which correspond to voids developing between the W nano-grains and/or amorphous regions. As a consequence, a large difference was observed in the structure of the Cu-on-W and the W-on-Cu interface, even though both were wavy. As shown in Figs. 2(d) and 3(d), the W-on-Cu interface appeared sharp and chemically abrupt, while the Cu-on-W interface displayed more roughness owing to the nano-fibrous W structure and the local roughness associated with it.

Cross-sectional TEM selected area electron diffraction patterns (Fig. 4) for (a) $\Lambda = 10$ nm and (b) $\Lambda = 60$ nm indicate that Cu and W layers display a nanocrystalline structure, with no clear preferred growth orientation. The Cu/W layers grew incoherently in both cases. The W diffraction rings were practically continuous, while the Cu rings were formed by discrete spots. Therefore, the W nanograins were on average much finer than the Cu ones. Additionally, the grain sizes in all cases seemed to scale with the layer thickness, as they were in general smaller in the 10 nm multilayer than in the 60 nm multilayers.

Fig. 5 shows TEM images for the Cu/W multilayer with $\Lambda = 10$ nm. The W layers appear darker in this imaging mode due to mass-thickness contrast. The bright-field (BF) image in Fig. 5(a) shows that the columnar nano-grains in the W layers are very thin, 1–3 nm thick, while the Cu layers consisted of grains about 5 nm thick and 15 nm wide. Fig. 5(b) also shows the voids developed at the columnar boundaries, as indicated by the white arrows, as shown before. For the case $\Lambda = 60$ nm, Fig. 6 shows the corresponding BF images at higher magnification. The Cu layers display mostly equiaxed grains that are much bigger (up to 50 nm) than for the case $\Lambda = 10$ nm; moreover the presence of some nanotwins is also observed, as indicated by the white arrows. The W layers were in turn composed of irregular, mostly columnar nanocrystals 3 to 5 nm wide and up to 30 nm thick, separated by very thin boundaries appearing as white veins (Fig. 6b), which correspond to voids and/or amorphous regions aligned with the growth direction.

3.2. Room temperature hardness and elastic modulus

The measurements of the hardness and elastic modulus of the Cu/W multilayers were challenging due to the large surface roughness of the coatings. The variation of hardness and elastic modulus is plotted in Fig. 7 as a function of normalized contact depth (ratio of contact depth, h_c to coating thickness, t_c). The increased scatter at low depths ($h_c/t_c < 0.1$) is due to tip rounding and surface roughness effects. Data at $h_c/t_c < 0.1$ lie outside the range recommended by the instrumented nanoindentation standard ISO14577 p4 to obtain reproducible hardness values. According to this standard, h_c should be more than 20 times the average surface roughness of the film, R_a, in order to minimize uncertainties in the determination of the contact areas. From the R_a of the Cu/W multilayers (given in Table 1), h_c should be at least 120 nm ($h_c/t_c > 0.1$) for Cu/W 5/5 nm and 15/15 nm multilayers and even larger, 160 nm ($h_c/t_c > 0.16$) for Cu/W 30/30 nm, with $R_a > 8$ nm. Since some substrate effects were expected at the recommended indentation depths, the hardness and elastic moduli were finally determined from a linear fit extrapolation to $h_c/t_c = 0$ in the range $0.1 < h_c/t_c < 0.25$, as shown in Fig. 7 and summarized in Table 1.

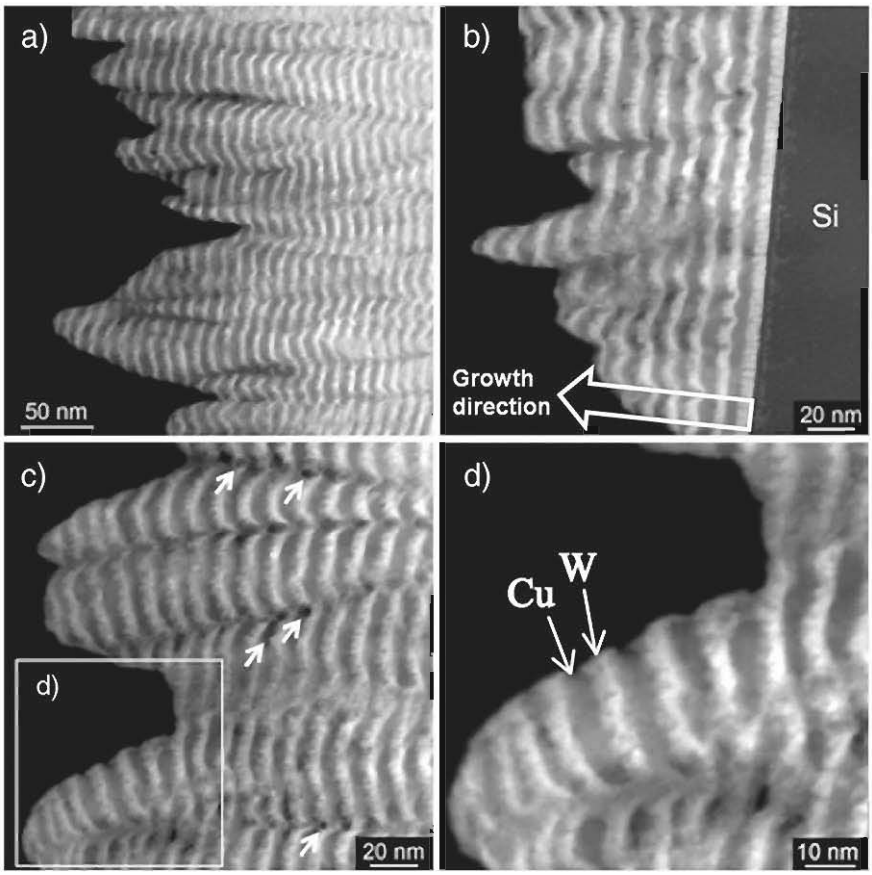

Fig. 2. STEM-HAADF images of the Cu/W multilayer with $\Lambda = 10$ nm. Arrows point out regions with low density/scattering power, most probably cavities (c).

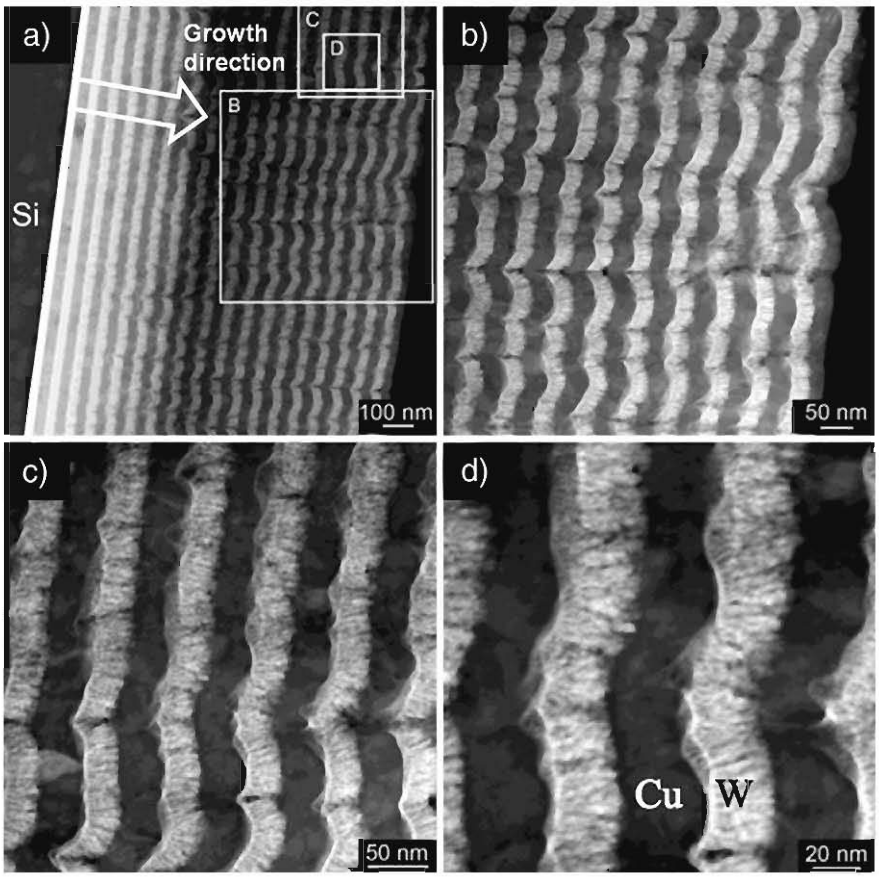

Fig. 3. STEM-HAADF images of the Cu/W multilayers with $\Lambda = 60$ nm.

It is clear from Fig. 7 that the hardness of these Cu/W multilayers was not strongly dependent on the modulation periodicity. The hardness was ≈5.2 GPa, within the experimental scatter, when Λ varied between 10 and 60 nm. Moreover, the hardness was not above the hardness given by the rule-of-mixtures for sputtered Cu and W, whose typical hardness is of the order of 2–3 GPa [24] and 15 GPa [25], respectively. Therefore, the multilayer structure did not seem to add any additional strengthening in the case of the Cu/W multilayers, as opposed to the behavior found in other fcc/bcc NMMs, like Cu/Nb, where hardness was well above the rule of mixtures of the constituents.

The elastic modulus did show some dependency on the modulation periodicity, increasing from 137 GPa to 163 GPa, when Λ increased from 10 to 60 nm. This was unexpected as the elastic moduli of NMMs typically lie within the rule of mixtures composite modulus of the constituents. It should be noted that these moduli are far below the predictions obtained from the rule of mixtures for bulk Cu ($E \approx 120$ GPa) and W ($E \approx 395$ GPa). There are several reasons why the multilayers might display a lower elastic modulus than expected, as will be discussed in more detail in Section 4.

Finally, indentation imprints were imaged by AFM immediately after indentation to ensure that the results were not compromised by errors associated with pile-up/sink-in effects in the estimation of the contact area using the Oliver and Pharr method [25]. Typical 2D scans of residual indents performed at 2 mN are shown in Fig. 8. Some piling-up of indented material was visible around the indentations but no shear bands occurred. The scans show the problem of indenting at low penetration

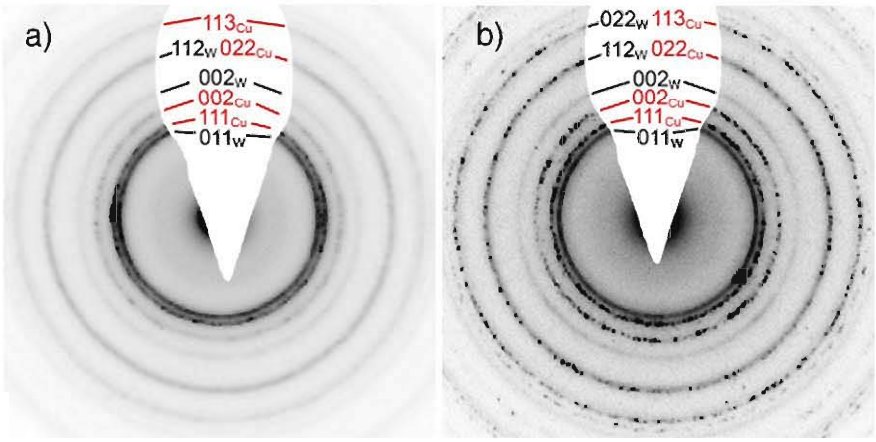

Fig. 4. Selected area electron diffraction patterns of the Cu/W multilayers: (a) Cu/W 5/5 nm and (b) Cu/W 30/30 nm.

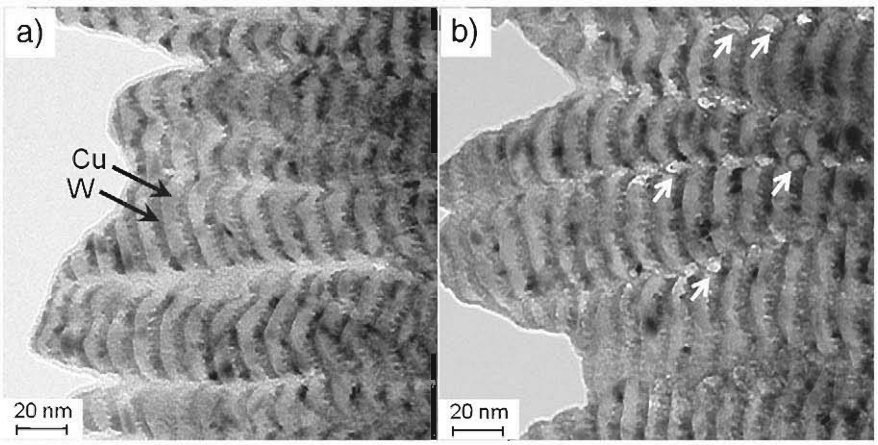

Fig. 5. (a) BF image of the 5/5 nm Cu/W multilayers showing smaller columnar grains in darker W layers. (b) Another area showing few voids (marked with arrows) at the columnar boundaries.

depths, associated with the waviness/roughness of the layers. The 2 mN indent, with $h_c \approx 100$ nm, performed in the Cu/W multilayer with $\Lambda = 60$ nm, characterized by $R_a \approx 8$ nm, was hardly distinguishable from the rough surface topography, as seen in Fig. 8(c). This observation justifies the strategy followed to obtain the hardness of the multilayers by discarding all indentations with $h_c < 20\,R_a$ and extrapolating the hardness to $h_c = 0$. In any case, the hardness values determined from the direct measurement of the projected areas (A_p) in the AFM scans, as $H = F/A_p$, where F is the indentation load, showed an excellent agreement with the hardness values determined from the Oliver and Pharr method and plotted in Fig. 7, demonstrating the validity of the approach.

The morphology of the pile-ups was not comparable to the smooth pile-up typically found during indentation of bulk, low strain-hardening metals. On the contrary, the pile-up morphology indicates a severe disruption of the columnar microstructure which is connected to the waviness of the multilayers. This explains why the degree of pile-up increased with the modulation periodicity, as also observed for the waviness and the apparent level of voids at the columnar boundaries.

3.3. Hot hardness

The hardness of the Cu/W NMMs is plotted as a function of indentation temperature in Fig. 9(a). As expected, hardness drops with temperature due to the thermally activated nature of plastic deformation, as previously observed in hot nanoindentation of thin metallic films [26]. Two major observations could be drawn from these data. First, as reported for the room temperature hardness, the modulation periodicity had no effect on the hot hardness. Secondly, the reduction in hardness with temperature was much larger than that reported recently [27] in Cu/Nb, another fcc/bcc NMM, which is plotted in Fig. 9(b) for comparison. In analyzing hot hardness results, it is useful to consider that high temperature deformation is often described using a phenomenological equation of the form:

$$\dot{\varepsilon} = A\sigma^n exp\left(\frac{-Q}{RT}\right) \tag{1}$$

where A is a constant, $\dot{\varepsilon}$ is the strain rate, σ is the flow stress, R is the universal gas constant and Q and n are the activation energy and stress exponent, respectively, for the rate-controlling deformation mechanism. Since the indentations were performed at a prescribed loading rate, and considering H proportional to the flow stress, Eq. (1) can be modified:

$$H = H_0 exp\left(\frac{Q/n}{RT}\right) \tag{2}$$

where H_0 can be interpreted as the extrapolated hardness at 0 K. Based on Eq. (2), a hardness versus 1/T plot can be very instructive to identify changes in deformation mechanisms from the hardness drop with T. For instance, Fig. 9(c) and (d) re-plots the hardness data for Cu/W and Cu/Nb NMMs respectively, versus 1/T. In the case of Cu/Nb, the H

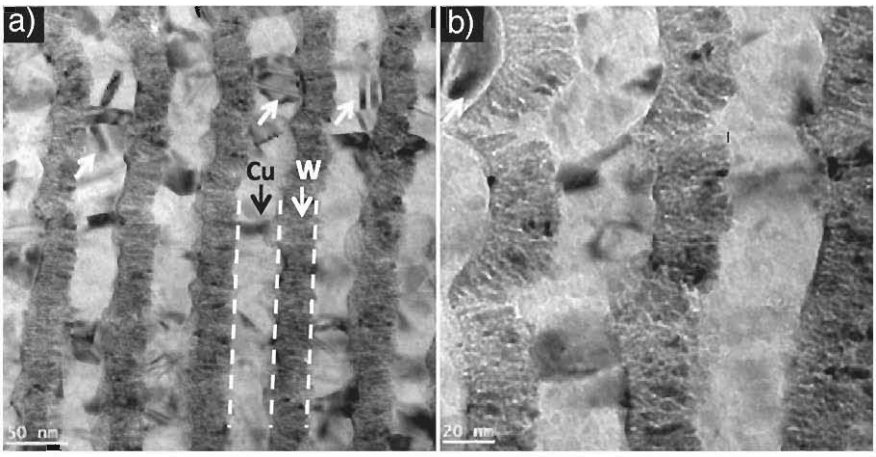

Fig. 6. BF images of the 30/30 nm Cu/W multilayers: (a) general view showing larger grains in Cu layers with numerous nanotwins (arrows). (b) Details of the white veins in the W layers corresponding to aligned voids and amorphous regions.

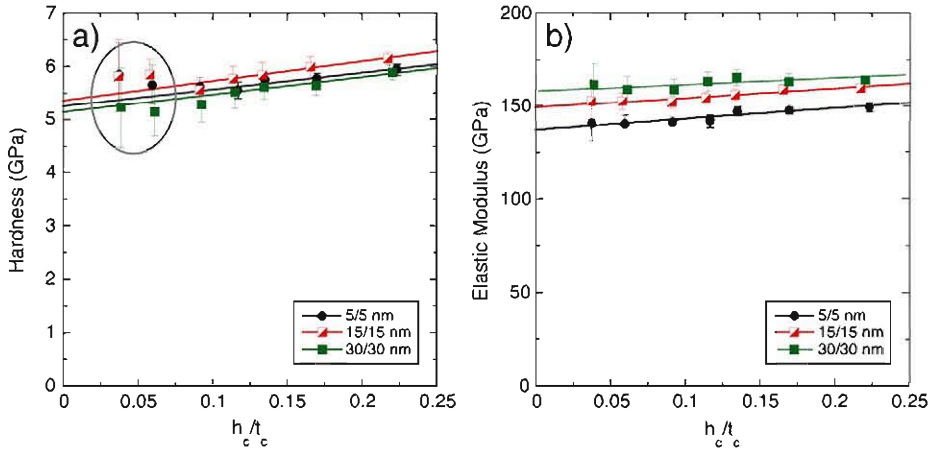

Fig. 7. (a) Hardness (H) and (b) elastic modulus (E) of the Cu/W multilayers as a function of normalized contact depth (hc/tc). The dashed circle contains data influenced by the coating roughness and the solid lines represent linear fits of the data at 0.1 < hc/tc < 0.25, from which H and E were determined by extrapolation to $h_c/t_c = 0$.

vs. 1/T slopes were constant for each modulation, indicating no changes in deformation mechanism between RT and 300 °C. Additionally, the multilayers retained a considerable hardness up to 300 °C, which corresponds to a homologous temperature for Cu of 0.4. Finally, the hardness reduction with temperature showed some weak dependency on the modulation, with the 5/5 nm multilayer retaining a higher hardness fraction with temperature. On the contrary, the Cu/W NMMs did not show any of these features. The hardness reduction with temperature followed a similar trend that for Cu/Nb multilayers up to 200 °C, but it increased at higher temperatures, indicating a change in deformation mechanism. As a result, the multilayer hardness at 300 °C was very small. Moreover, all Cu/W NMMs showed the same behavior with temperature, regardless of modulation periodicity. In order to get more information about the high temperature deformation behavior, some of indents were cross-sectioned using FIB. Fig. 10 shows a SEM cross-sectional image of a 2 mN indent performed on the 30/30 nm Cu/W multilayer at T = 350 °C. The inset shows an STEM-HAADF image of the area immediately under the indent. The layered structure shows that deformation was localized on the Cu layers which exhibited severe thinning compared with the W layers, possibly indicating that Cu is infiltrating into the W porous layers under the indenter, presumably by temperature assisted plastic flow.

4. Discussion

Overall, the nanoindentation results indicate that the Cu/W NMMs under study do not show the strengthening behavior observed in other fcc/bcc NMMs like Cu/Nb. There is clear evidence that the controlling strengthening mechanism in Cu/Nb NMMs is the interaction between dislocations and interfaces [28,29]. The fact that the hardness of the Cu/W multilayers is independent of modulation periodicity indicates that the strength in this case is not controlled by the Cu/W interfaces. This is surprising because it was expected that the interfaces in Cu/W should become a large obstacle to dislocation glide due to the large elastic and lattice mismatch [16] between Cu and W, which is larger than between Cu and Nb. Moreover, the more refractory character of W over Nb (melting points are 3400 °C and 2470 °C respectively [30]) led to foresee a higher hot hardness as well, which is opposed to the results in Fig. 9.

Table 1
Hardness, elastic modulus and surface roughness of the Cu/W multilayers.

Sample	Hardness (GPa)	Elastic modulus (GPa)	Roughness, R_a (nm)
5/5 nm	5.2 ± 0.2	137 ± 5	3 ± 0.2
15/15 nm	5.3 ± 0.2	150 ± 5	3.2 ± 0.2
30/30 nm	5.1 ± 0.2	163 ± 5	8.5 ± 0.4

The microstructural differences reported above between Cu/Nb and Cu/W multilayers may be the reason behind the discrepancies observed in mechanical properties. PVD deposited Cu/Nb multilayers also developed some layer waviness within the film thickness, similar to that found in Cu/W multilayers. However, Cu/Nb NMMs typically display a marked growth texture, with Cu and Nb growing preferentially in the [111] and [110] orientations, respectively [31]. As a result, Cu/Nb multilayers present abrupt interfaces with a Kurdjumov–Sachs (KS: $\{111\}_{Cu}//\{110\}_{Nb}$ and $<110>_{Cu}//<111>_{Nb}$) orientation relationship. This type of interface has low shear strength and represents a large obstacle to dislocation glide [32]. In addition, both the Cu and Nb layers typically contain one single-grain along the layer thickness, which is usually smaller than the in-plane grain size.

On the contrary, the Cu/W multilayers presented in this paper show a very different microstructure, as describe in Section 3.1. The main differences can be attributed to the low homologous temperature of W during deposition, implying low mobility of the W adatoms, as summarized below. First, the Cu/W NMMs do not show any preferred texture (Fig. 4) and, consequently, Cu and W do not grow with any predominant interface character. Moreover, the in-plane grain size in the W layers is much smaller than in the Cu layers, as shown in Figs. 5 and 6, and this indicates that the underlying layer does not determine the nucleation of the subsequent layer through heteroepitaxy. Secondly, even though the Cu layers appear dense with a grain structure similar to that encountered in Cu/Nb NMMs, the W layers show a fibrous structure with some voids in the columnar boundaries between the nanograins, as shown in Figs. 3 to 6. Finally, there is a large asymmetry in the structure of the Cu-on-W and the W-on-Cu interface, as reported previously [33]. As shown in Figs. 2(d) and 3(d), the W-on-Cu interface appeared sharp and chemically abrupt, while the Cu-on-W interface appeared jagged due to the fibrous W structure and the local roughness that developed. It is actually feasible to imagine that Cu atoms can easily diffuse into the porous boundaries ("veins") between the W nanograins due the higher Cu mobility during deposition.

The morphology of the W layers as well as the potential layer intermixing discussed above is the most plausible explanation for the negligible effect of the periodicity on the hardness of Cu/W NMMs. Moreover, the elastic modulus of the Cu/W NMMs decreases with periodicity, with values well below the expected rule of mixtures assuming

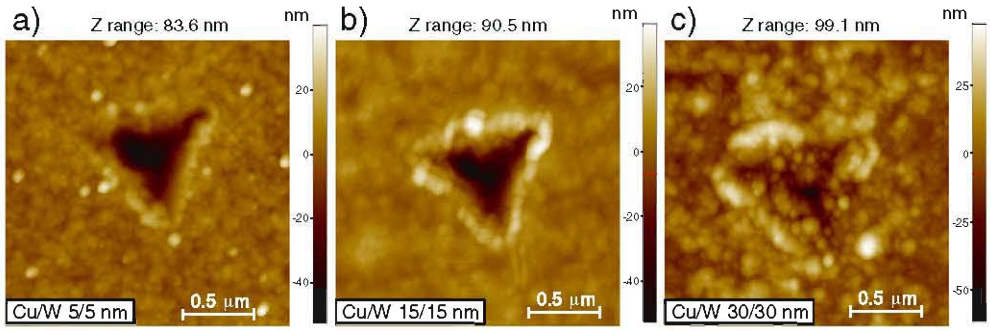

Fig. 8. AFM topography scans ($2.5 \times 2.5\ \mu m^2$) of residual indents performed with loads of 2 mN for: (a) Cu/W 5/5 nm, (b) Cu/W 15/15 nm and (c) Cu/W 30/30 nm multilayers.

the bulk modulus of Cu ($E_{Cu} = 120$ GPa) and W ($E_W = 395$ GPa). This might be due to the fact that the effective thickness of the W layers is reduced by the jagged Cu-on-W interface (estimated to have a thickness of 1–2 nm from Figs. 2(d) and 3(d)) and to the contribution of the intercolumnar porosity observed in Fig. 5. Finally, the dramatic hardness drop with temperature of Cu/W above 200 ºC (Fig. 9), not observed in Cu/Nb, is a consequence of temperature assisted Cu plastic infiltration into the W porous layers below the indenter, as evidenced from Fig. 10. In view of these results, future efforts on the development of Cu/W multilayers should concentrate on optimization of the W deposition parameters via substrate heating and/or ion assisted deposition to increase the W adatom mobility during deposition.

5. Conclusions

We deposited Cu/W NMMs by magnetron sputtering, with layer thickness ranging between 5 and 30 nm. The results showed that, contrary to Cu/Nb NMMs, the dependence of the hardness on the layer thickness was weak and the hardness dropped rapidly with temperature, especially above 200 ºC, as a consequence of the temperature assisted Cu plastic infiltration into the W layers. The results are attributed to the morphology of the W layers as well as to the reduction of the effective thickness for the W layer due to the roughness of the Cu on W interface, as revealed by TEM. Therefore, future efforts on the development of Cu/W multilayers should concentrate on optimization

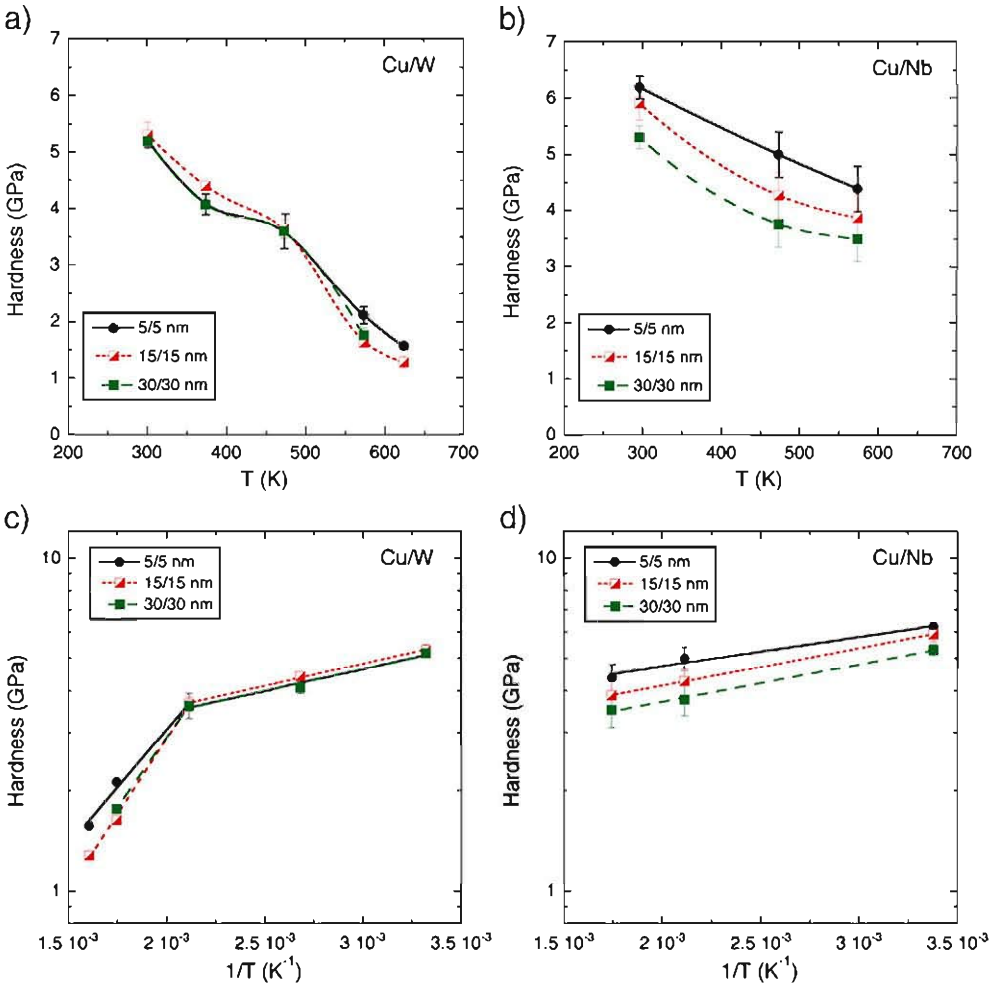

Fig. 9. Indentation hardness as a function of temperature for (a) Cu/W multilayers with periodicities $\Lambda = 10$ nm, 30 nm and 60 nm and (b) Cu/Nb multilayers with the same periodicities $\Lambda = 10$ nm, 30 nm and 60 nm [27]; Panels (c) and (d) show the corresponding Arrhenius plots from which the apparent activation energies for hardness were calculated.

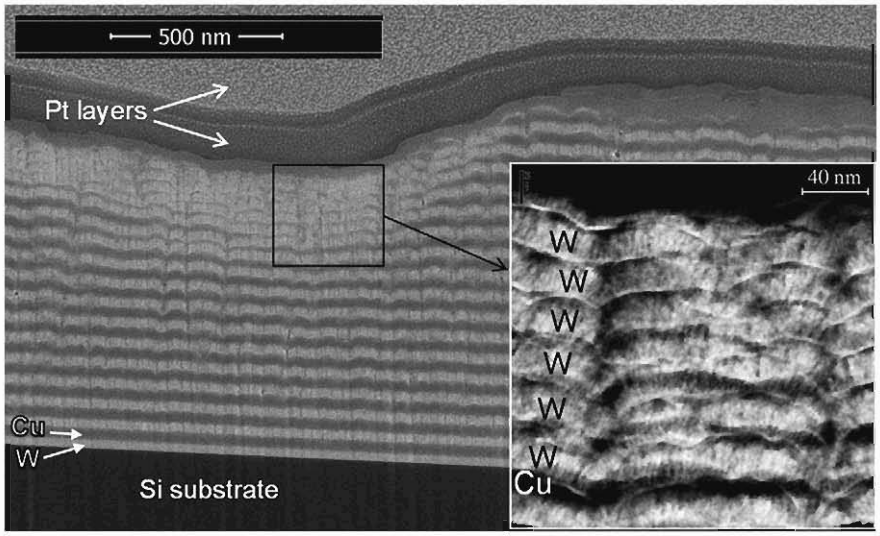

Fig. 10. SEM cross-sectional image of the indents in the Cu/W 30/30 nm multilayer tested at T = 350 °C. The Pt layers are protective layers deposited prior to ion milling the cross-section. The inset corresponds to an STEM-HAADF image of the area immediately below the indent.

of the W deposition parameters via substrate heating and/or ion assisted deposition to increase the W adatom mobility during deposition.

Acknowledgments

This investigation was supported by the European Commission through the project RADINTERFACES (Grant Agreement Number 263273). Additional support from the Spanish Ministry of Economy and Competitiveness (MAT2012-31889) is also gratefully acknowledged. M. K. would like to give appreciation for the possibility to use transmission electron microscope at the Institute of Physics of the Czech Republic in Prague financed under the project MEYS LM2011026.

References

[1] S.I. Rao, P.M. Hazzledine, Atomistic simulations of dislocation–interface interactions in the Cu–Ni multilayer system, Phil. Mag. A 80 (2000) 2011.
[2] R.G. Hoagland, T.E. Mitchell, J.P. Hirth, H. Kung, On the strengthening effects of interfaces in multilayer fcc metallic composites, Phil. Mag. A 83 (2002) 643.
[3] B. Shoykhet, M.A. Grinfeld, P.M. Hazzledine, Internal stresses and strains in coherent multilayers, Acta Mater. 46 (1998) 3761.
[4] B.J. Daniels, W.D. Nix, B.M. Clemens, Enhanced mechanical hardness in compositionally modulated Fe(001)/Pt(001) and Fe(001)/Cr(001) epitaxial thin-films, Thin Solid Films 253 (1994) 218.
[5] J.S. Koehler, Attempt to design a strong solid, Phys. Rev. B 2 (1970) 547.
[6] D.J. Bacon, D.M. Barnett, R.O. Scattergood, Anisotropic elastic field of a dislocation segment in 3 dimensions, Phil. Mag. A 39 (1979) 231.
[7] X. Chu, S.A. Barnett, Model of superlattice yield stress and hardness enhancements, J. Appl. Phys. 77 (1995) 4403.
[8] A. Misra, J.P. Hirth, H. Kung, Single-dislocation-based strengthening mechanisms in nanoscale metallic multilayers, Phil. Mag. A 82 (2002) 2935.
[9] P.M. Anderson, T. Foecke, P.M. Hazzledine, Dislocation-based deformation mechanisms in metallic nanolaminates, MRS Bull. 24 (1999) 27.
[10] P.M. Anderson, J.S. Carpenter, Estimates of interfacial properties in Cu/Ni multilayer thin films using hardness data, Scr. Mater. 62 (2010) 325.
[11] F. Ren, S. Zhao, W. Li, B. Tian, L. Yin, A.A. Volinsky, Theoretical explanation of Ag/Cu and Cu/Ni nanoscale multilayers softening, Mater. Lett. 65 (1) (2011) 119.
[12] A. Misra, J.P. Hirth, R.G. Hoagland, Length-scale-dependent deformation mechanisms in incoherent metallic multilayered composites, Acta Mater. 5 (18) (2005) 4817.
[13] I. Smid, M. Akiba, G. Vieider, L. Ploch, Development of tungsten armour and bonding to copper for plasma-interactive components, J. Nucl. Mater. 258–263 (1998) 160.
[14] J. Esteve, G. Zambrano, C. Rincon, E. Martinez, H. Galindo, P. Prieto, Mechanical and tribological properties of tungsten carbide sputtered coatings, Thin Solid Films 373 (2000) 282.
[15] A.R. Miedema, Heat of formation of alloys, Philips Tech. Rev. 36 (1976) 217.
[16] M.J. Demkowicz, R.G. Hoagland, J.P. Hirth, Interface structure and radiation damage resistance in Cu–Nb multilayer nanocomposites, Phys. Rev. Lett. 100 (2008) 136102.
[17] Y. Gao, T. Yang, J. Xue, S. Yan, S. Zhou, Y. Wang, D.T.K. Kwok, P.K. Chu, Y. Zhang, Radiation tolerance of Cu/W multilayered nanocomposites, J. Nucl. Mater. 413 (2011) 11.
[18] L. Wang, W. Qi-Qi, C. Shun-Li, Z. Jing-Jun, A. Zhu, W. Yuan, Helium effect on the stability of the interface of Cu/W nanomultilayer, Acta Phys. Sin. 61 (2012) 176802.
[19] C. Wang, P. Brault, C. Zaepffel, J. Thiault, A. Pineau, T. Sauvage, Deposition and structure of W–Cu multilayer coatings by magnetron sputtering, J. Phys. D 36 (2003) 2709.
[20] J.W. Davis, K.T. Slattery, D.E. Driemeyer, M.A. Ulrickson, Use of tungsten coating on iter plasma facing components, J. Nucl. Mater. 233–237 (1996) 604.
[21] S.P. Wen, R.L. Zong, F. Zeng, Y. Gao, F. Pan, Evaluating modulus and hardness enhancement in evaporated Cu/W multilayers, Acta Mater. 55 (2007) 345.
[22] P. Villain, D. Faurie, P.O. Renault, E.L. Bourhis, P. Goudeau, K.F. Badawi, Mechanical properties and size effect in nanometric W/Cu multilayers, MRS Symp. Proc, 875, 2005, (OI 3.1–3.6).
[23] W.C. Oliver, G.M. Pharr, An improved technique for determining hardness and elastic modulus using load and displacement sensing indentation experiments, J. Mater. Res. 7 (1992) 1564.
[24] V. Srinivasarao, R. Jayaganthan, V.N. Sekhar, K. Mohankumar, Nanoindentation study of the sputtered Cu thin films for interconnect applications, Proc. 6th Electr. Pack. Technol. Conf., 2004, p. 343.
[25] L.N. Zhu, G.L. Li, H.D. Wang, B.S. Xu, D.M. Zhuang, J.J. Liu, Microstructures and nano mechanical properties of the metal tungsten film, Curr. Appl. Phys. 9 (2009) 510.
[26] A.A. Volinsky, N.R. Moody, W.W. Gerberich, Nanoindentation of Au and Pt/Cu thin films at elevated temperatures, J. Mater. Res. 18 (2004) 2650.
[27] M.A. Monclus, S.J. Zheng, J.R. Mayeur, I.J. Beyerlein, N.A. Mara, T. Polcar, J. LLorca, J.M. Molina-Aldareguía, Optimum high temperature strength of two-dimensional nanocomposites, APL Mater. 1 (2013) 052103.
[28] J.J. Niu, J.Y. Zhang, G. Liu, P. Zhang, S.Y. Lei, G.J. Zhang, J. Sun, Size-dependent deformation mechanisms and strain-rate sensitivity in nanostructured Cu/X (X = Cr, Zr) multilayer films, Acta Mater. 60 (2012) 3677.
[29] R.F. Zhang, J. Wang, I.J. Beyerlein, T.C. Germann, Dislocation nucleation mechanisms from fcc/bcc incoherent interfaces, Scr. Mater. 65 (2011) 1022.
[30] http://www.engineeringtoolbox.com/melting-temperature-metals-d_860.html .
[31] K.Y. Zhang, J.D. Embury, K. Han, A. Misra, Transmission electron microscopy investigation of the atomic structure of interfaces in nanoscale Cu–Nb multilayers, Phil. Mag. 88 (2008) 2559.
[32] I.J. Beyerlein, N.A. Mara, J. Wang, J.S. Carpenter, S.J. Zheng, W.Z. Han, R.F. Zhang, K. Kang, T. Nizolek, T.M. Pollock, Structure–property-functionality of bimetal interfaces, JOM 64 (2012) 1192.
[33] F. Pan, S.P. Wen, R.L. Zong, F. Zeng, Y. Gao, Evaluating modulus and hardness enhancement in evaporated Cu/W multilayers, Acta Mater. 55 (2007) 345.